fuels

MDPI

Article

Non-Premixed Filtered Tabulated Chemistry: Filtered Flame Modeling of Diffusion Flames

Pedro Javier Obando Vega [1,2], Axel Coussement [1], Amsini Sadiki [2,3] and Alessandro Parente [1,*]

[1] Aero-Thermo-Mechanics Laboratory, École Polytechnique de Bruxelles, Université Libre de Bruxelles, Avenue F.D Roosevelt, 50–CP 165/41, 1050 Brussels, Belgium; obando@ekt.tu-darmstadt.de (P.J.O.V.); axcousse@ulb.ac.be (A.C.)

[2] Institute of Energy and Power Plant Technology, Technical University of Darmstadt, Otto-Berndt-Str. 3, 64287 Darmstadt, Germany; sadiki@ekt.tu-darmstadt.de

[3] Reactive Flows and Diagnostics, Technical University of Darmstadt, Otto-Berndt-Str. 3, 64287 Darmstadt, Germany

* Correspondence: alessandro.parente@ulb.be; Tel.: +32-(0)2-650-26-80

Abstract: The flame front filtering is a well-known strategy in turbulent premixed combustion. An extension of this approach for the non-premixed combustion context has been proposed by means of directly filtering counterflow diffusion flamelets. Promising results were obtained for the non-premixed filtered tabulated chemistry formalism on 1-D and 2-D unresolved counterflow flame configurations. The present paper demonstrates the soundness of this approach on a 3-D real laminar non-premixed coflow flame. The model results are compared against the direct filtering of the fully resolved laminar diffusion flame showing that the formalism adequately describes the underlying physics. The study reveals the importance of the one-dimensional counterflow flamelet hypothesis, so that the model activation under this condition is ensured by means of a flame sensor. The consistent coupling between the model and the flame sensor adequately retrieves the flame lift-off and satisfactorily predicts the profile extension due to the filtering process.

Keywords: laminar non-premixed combustion; coflow flame; filtered tabulated chemistry

Citation: Obando Vega, P.J.; Coussement, A.; Sadiki, A.; Parente, A. Non-Premixed Filtered Tabulated Chemistry: Filtered Flame Modeling of Diffusion Flames. *Fuels* **2021**, 2, 87–107. https://dx.doi.org/10.3390/fuels2020006

Academic Editor: Martin Olazar
Received: 6 January 2021
Accepted: 2 February 2021
Published: 25 March 2021

1. Introduction

Due to unceasing discoveries in the field of chemical kinetics the size of detailed chemical mechanisms has continuously augmented in recent last years [1]. Despite the increase of computational power, their application remains limited to specific academic combustion problems, and reduction techniques are unquestionably necessary in order to be able to simulate practical combustion problems.

Flamelet based methods assume thin flame structures with significantly smaller time scales compared to the flow. Exploiting this feature, the chemistry description can be parametrized in terms of few controlling variables resulting in significant computational time reduction [2]. Within this framework, FGM (Flamelet Generated Manifold) [3] and FPI (Flamelet Prolongation of Intrinsic Low Dimensional Manifolds) [4], both initially developed for premixed and afterwards extended to non-premixed regime, as well as FPV (Flamelet/Progress Variable) [5,6] method for non-premixed regime are consolidated techniques. Acknowledging their flexibility, further developments have permitted the assessment of highly specialized applications, e.g., ethanol spray combustion [7], where FGM is coupled with an ATF (Artificially Thickened Flame) [8] approach employing dynamic flame surface wrinkling, or oxy-flame combustion by means of FPV coupling with an stochastic fields methodology [9].

Different strategies exist to compute turbulent reacting flow problems depending on the level of resolution or modeling of the turbulence structures: Direct Numerical Simulations (DNS), Large Eddy Simulations (LES) and Reynolds Averaged Navier Stokes

(RANS). In DNS all turbulence scales are explicitly computed, in LES only the larger scale motions are resolved on the numerical grid and the smaller scale motions are accounted for by a subgrid scale (SGS) model [10], and in RANS only mean flow fields are resolved [11]. LES is a well developed approach [12] which offers a substantial decrease with respect to DNS [13], a non exhaustive list for the interested reader includes the work in [14–20]. The filtering or ensemble averaging of the balance equations, in LES and RANS respectively, gives origin to unclosed terms which are unknown and should be modeled [21]. Tackling premixed turbulent combustion, the FTACLES (Filtered Tabulated Chemistry for LES) combustion model [22] is based on the direct application of a filtering operator to one-dimensional laminar flamelets. The strategy to estimate the closure terms ensures both the correct flame propagation as well as the recovery of the chemical structure of the filtered flame. The formalism has been extended to partially premixed regimes [23] and heat loss effects [24].

Currently, work has been carried out regarding non-premixed flamelet filtering for LES. Two strategies have been proposed which differ in the way the flamelet modification through turbulence is taken into account. The approach followed in [25,26] derives the turbulent flamelet equation from the filtered species transport. Subsequently, similarity law and scaling relations in order to estimate the filtered chemical source term and scalar dissipation rate are proposed based on a-priori DNS study in [25], while [26] suggests a source term estimation employing first-order conditional moment closure.

Another way to tackle the problem is to directly filter the laminar flamelet and model the turbulence effect. Following this reasoning, the non-premixed filtered tabulated chemistry model as proposed in [27] has been designed to tackle turbulent combustion problems where the flame wrinkling is fully resolved or for laminar flame fronts. The model has been applied to 1-D and 2-D unresolved counterflow flame configurations. Coussement et al. report that the model appropriately captures the filtered flame thickness and filtered temperature profiles, for all the assessed filter sizes [27].

Though numerically alike, non-negligible differences exist from the theoretical point of view between the filtering of a diffusion flame front with respect to the premixed counterpart. Non-premixed flames do not possess neither a characteristic velocity scale nor a flame thickness defining a characteristic length scale [28]. Hence the flame thickness δ will not only depend on the composition but will change as well either as a function of time, for an unsteady evolving diffusion flame, or as a function of the strain rate K. For the latter it holds that $\delta \propto K^{-1/2}$, so that the flame thickness within a manifold spans several orders of magnitude. Consequently, the transformation caused by a given filter size Δ will significantly vary as a function of the filter-to-thickness ratio Δ/δ at every flamelet. It follows that while a diffusion flame front filtering operation can be clearly formulated from the numerical point of view, the conservation of a given property characterizing the flame is considerably more difficult to demonstrate.

The goal of the present study is to assess the capability of the non-premixed filtered tabulated chemistry formalism to adequately describe the filtered flame structure of a real diffusion flame. This is done by appraising the performance of the model over a coflow laminar non-premixed flame. On the previous work [27], the model satisfactorily performed on steady strained counterflow flame configurations, i.e., one fixed K value, however the application on a real configuration has not yet been explored. Even though the preceding results proved the mathematical soundness of the approach, the model assessment on a real diffusion flame is essential to unambiguously demonstrate that the formalism preserves the flame characteristic features and therefore adequately represents the underlying physics. More specifically, the computation of a real laminar flame decidedly increases the problem complexity as interactions between flamelets with considerably different filtering sensitivity might occur, contrary to the steady strained counterflow flame case where the problem was limited to the adequate description of one specific trajectory within the manifold, i.e., no flamelet interaction. Moreover, recalling that the ultimate objective of the model is to be employed in LES, this study is a necessary intermediate step

to substantiate the consistence of the formulation. Satisfactory results in this stage would then justify the further consideration of an efficiency function taking into account the modified interaction between the filtered flame front and the subgrid turbulent structures.

The structure of the paper is as follows: Section 2 is devoted to the presentation of the non-premixed filtered tabulated chemistry model and the description of the study case consisting on a laminar diffusion coflow flame. Section 3 presents first non-premixed filtered tabulated chemistry results and the reasons for the observed deviations are discussed. A model activation strategy employing a sensor S based on the flame dimensionality is proposed and the model's performance is assessed. Section 4 expands the model understanding considering the existence of conserved features in the filtered flame structure, and highlighting the fundamental role S plays on the non-premixed filtered tabulated chemistry model. Concluding remarks are presented in the last section.

2. Materials and Methods

In the first part of this section the non-premixed filtered tabulated chemistry concept is briefly introduced. The flamelet equations as expressed in the FGM context are presented, followed by the filtered governing equations for an adiabatic reactive flow coupled with a tabulated chemistry approach. The closure of the unresolved terms is addressed in accordance with the non-premixed filtered tabulated chemistry formalism. The second part of this section introduces the study case, the numerical setup and the chemical data base construction.

2.1. Flamelet Equations

The FGM approach is based on the idea that a multidimensional flame can be described in terms of one-dimensional structures called flamelets [3]. The reactive system is characterized by a set of slow processes, while the fast evolving ones are in a generalized steady state [2]. Exploiting this feature, the steady state manifold resulting from the solution of the flamelet equations is precomputed and parameterized a function of the slow evolving controlling variables. Thus, exclusively the transport equations for the parameterizing variables are solved during the flame simulation, and the remaining flame variables are retrieved from the lookup table, resulting into a substantial reduction of the computational time [29]. The flamelet equations [30] are one-dimensional expressions which describe mass, species and energy conservation in a flame adapted coordinate system

$$\frac{\partial \rho u}{\partial s} + \rho K = 0\,, \tag{1}$$

$$\frac{\partial \rho u Y_i}{\partial s} + \rho K Y_i = \frac{1}{Le_i}\frac{\partial}{\partial s}\left(\frac{\lambda}{c_p}\frac{\partial Y_i}{\partial s}\right) + \dot{\omega}_{Y_i}\,, \tag{2}$$

$$\frac{\partial \rho u h}{\partial s} + \rho K h = \frac{\partial}{\partial s}\left[\frac{\lambda}{c_p}\frac{\partial h}{\partial s} + \sum_{1=1}^{N_s} h_i \frac{\lambda}{c_p}\left(\frac{1}{Le_i} - 1\right)\frac{\partial Y_i}{\partial s}\right], \tag{3}$$

where s is the spatial coordinate perpendicular to the flame front, ρ the mass density, u the velocity, K the flame stretch rate, Y_i the mass fraction of species i, and h the enthalpy. Le_i is the Lewis number of species i, λ the thermal conductivity, c_p the specific heat at constant pressure, $\dot{\omega}_{Y_i}$ the chemical production rate, and N_s the total number of species.

The counterflow flame configuration can be used to describe diffusion flames, where the two dimensional flow field effects are taken into account through the local stretch rate K [31]. Thus a transport equation for the stretch field is solved [32]

$$\frac{\partial \rho u K}{\partial s} = \frac{\partial}{\partial s}\left(\frac{\mu \partial K}{\partial s}\right) - 2\rho K^2 + \rho_2 a^2\,, \tag{4}$$

where a is the applied strain rate s^{-1} and ρ_2 the density, both at the oxidizer stream.

The mixture fraction Z is obtained from the transport of a passive scalar with the assumption of Le equal to unity

$$\frac{\partial \rho u Z}{\partial s} + \rho K Z = \frac{\partial}{\partial s}\left(\frac{\lambda}{c_p}\frac{\partial Z}{\partial s}\right), \tag{5}$$

The progress variable c is defined as a linear combination of chemical species

$$c = \sum \gamma_i Y_i, \tag{6}$$

where γ_i is a weight factor.

The solution of the flamelet equations at varying K generates a non-premixed low-dimensional manifold. For an adiabatic condition the thermodynamical and chemical properties can be uniquely parameterized as $\Phi = f(Z, c)$.

2.2. Filtered Reactive Flow Governing Equations

In the tabulated chemistry context, a reactive flow can be described solving the parameterizing variables transport equations together with the continuity and momentum equations. Applying a filtering operation, as it would be in the LES context, for an adiabatic condition, and assuming $Le = 1$, the resulting system reads

$$\frac{\partial \bar{\rho}}{\partial t} + \nabla \cdot (\bar{\rho}\tilde{\mathbf{u}}) = 0, \tag{7}$$

$$\frac{\partial \bar{\rho}\tilde{\mathbf{u}}}{\partial t} + \nabla \cdot (\bar{\rho}\tilde{\mathbf{u}}\tilde{\mathbf{u}}) = \nabla \cdot \bar{\tau} - \nabla \bar{p} + \Omega_u, \tag{8}$$

$$\frac{\partial \bar{\rho}\tilde{Z}}{\partial t} + \nabla \cdot (\bar{\rho}\tilde{\mathbf{u}}\tilde{Z}) = \nabla \cdot (\rho_0 D_0 \nabla \tilde{Z}) + \Omega_Z + \alpha_Z, \tag{9}$$

$$\frac{\partial \bar{\rho}\tilde{c}}{\partial t} + \nabla \cdot (\bar{\rho}\tilde{\mathbf{u}}\tilde{c}) = \nabla \cdot (\rho_0 D_0 \nabla \tilde{c}) + \overline{\dot{\omega}}_c + \Omega_c + \alpha_c, \tag{10}$$

where $\bar{\cdot}$ and $\tilde{\cdot}$ correspond to the Reynolds or spatial filter and the Favre or mass-weighted spatial filter, respectively. τ the laminar viscous tensor, p the pressure, and Ω_u is the momentum unresolved laminar convective contribution, and can be neglected as demonstrated in [27]. D is the molecular diffusivity, ρ_0 and D_0 reference values for the density and the molecular diffusion coefficient. $\overline{\dot{\omega}}_c$ is the unresolved chemical production term, and employing φ for the parameterizing variables Z and c, Ω_φ and α_φ are the unresolved convective and diffusive contributions:

$$\Omega_\varphi = -\nabla \cdot (\overline{\rho \mathbf{u} \varphi} - \bar{\rho}\tilde{\mathbf{u}}\tilde{\varphi}), \tag{11}$$

$$\alpha_\varphi = \nabla \cdot (\overline{D \nabla \varphi} - \bar{D} \nabla \tilde{\varphi}). \tag{12}$$

2.3. Non-Premixed Filtered Tabulated Chemistry Closure

The non-premixed filtered tabulated chemistry formalism is based on the idea that if there is no SGS wrinkling, Equations (11) and (12), as well as the unresolved chemical production can be estimated by directly filtering the one-dimensional flamelet solutions. A Gaussian filter, corresponding to the Gaussian distribution with mean zero and variance $\sigma^2 = \frac{1}{12}\Delta^2$ [14], is then employed

$$F(r_x) = \left(\frac{6}{\pi \Delta^2}\right)^{1/2} exp\left(-\frac{6 r_x^2}{\Delta^2}\right). \tag{13}$$

where Δ is the filter size, $r_x = x - x_0$ the spatial lag-distance. For the non-premixed regime the computation of these terms has been carefully addressed by Coussement assuming the flame structure to be similar to a planar filtered counterflow flame at a given strain rate [27].

The velocity vector **u** is decomposed into the velocity of the flame front (localized on a given iso-Z and constant over the flame) and the local velocity in the flame front. Referring to the flamelet solutions with the symbol *, Equation (11) can be expressed in terms of the contributions in flame front local coordinates as:

$$\Omega_\varphi = \frac{\partial}{\partial s}\left(\overline{\rho^* u^* \varphi^*} - \bar{\rho}^* \tilde{u}^* \tilde{\varphi}^*\right) + \left(\overline{\rho^* K^* \varphi^*} - \bar{\rho}^* \tilde{K} \tilde{\varphi}^*\right), \tag{14}$$

where u and K are the variables defined in the flamelet equations. Considering the vector normal to the flame front $n = \nabla\tilde{Z}/|\tilde{Z}|$, and assuming that ∇Z and $\nabla\varphi$ are aligned according to [25], the diffusive term becomes:

$$\alpha_\varphi = \nabla \cdot \left[\overline{\rho^* D^* \frac{\partial \varphi^*}{\partial s} sign\left(\frac{\partial Z^*}{\partial s}\right) n}\right] - \nabla \cdot \left[\rho_0^* D_0^* \frac{\partial \tilde{\varphi}^*}{\partial s} sign\left(\frac{\partial \tilde{Z}^*}{\partial s}\right)\right]. \tag{15}$$

Details about the derivation can be found in [27].

2.4. Coflow Flame Configuration

A laminar coflow methane-air diffusion flame numerically analyzed in [33] has been simulated to assess the model performance in absence of turbulence. The burner configuration consists of a central fuel jet with a mixture composition of 55% CH_4 and 45% N_2 in molar fractions, surrounded by an air coflow. The jet's inner radius is $r_{Fuel} = 6$ mm, the outer coaxial tube has a radius of $r_{Air} = 27.5$ mm, and the domain length is 90 mm. The fuel velocity is defined by a parabolic profile, where $u_{max} = 0.23$ m/s, for the coflow air a plug flow with a constant velocity equal to the maximum fuel velocity is employed, and the side wall, i.e., $r = r_{Air}$ is set to no-slip. These conditions lead to a lifted flame as shown in Figure 1a which reproduces the finding in [33].

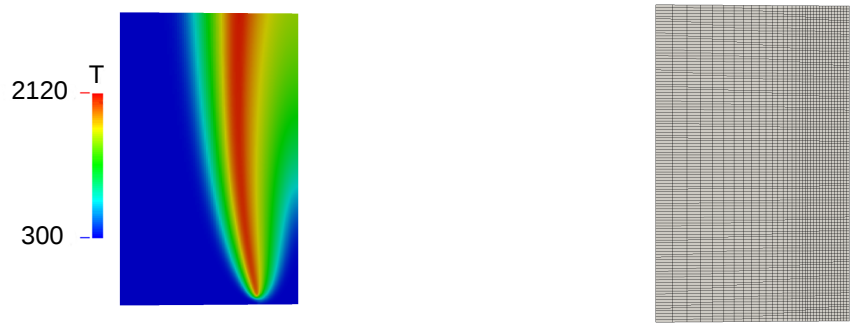

(**a**) (**b**)

Figure 1. Diffusion lifted flame temperature field (**a**) and representation of the numerical grid (**b**).

The filtering operation extends the flame in all directions, thus for a lifted condition the initial mixing zone will be reduced as the ignited structure expands upstream. The choice of this configuration is particularly challenging, for the method should correctly locate the ignition point, which is not fixed but will slightly vary as a function of the employed filter size. Moreover, for this case the influence of preferential diffusion on mixture fraction transport appears to be negligible [33], being the mixture composition a quite convenient feature.

2.5. Numerical Setup

The filtered tabulated chemistry model is implemented in the open source computational fluid dynamics (CFD) code OpenFOAM 2.4.0 following a low-Mach approach according to [34]. A Semi Implicit Methods Pressure Linked Equations (SIMPLE) algorithm [35] is applied for solving velocity, pressure and the parameterizing scalars. The convective term is discretized with a bounded second order central differencing

scheme, to improve the convergence for steady-state cases [36]. A second order, conservative scheme is employed for the the spatial discretization of the Laplacian terms.

The numerical grid is two-dimensional, axisymmetric, structured, constantly spaced along the axial direction, while radially a uniform spacing is employed for $r \leq r_{Fuel}$ and outwardly increasing cell size is used for $r_{Fuel} < r < r_{Air}$. Three different refinement levels are used. $NU1$ is a finer mesh than the one used in [33], which proved to have an appropriate resolution. Systematic coarsening, with an increasing factor $F \approx 2$ in each direction is applied to obtain $NU2$ and $NU3$. The grid details are indicated on Table 1.

Table 1. Numerical grid parameters. $\Delta_{x,st}$ is the average cell size at the stoichiometric condition throughout the domain $\Delta_{x,st} = \langle \Delta_x | Z = Z_{st} \pm 0.01 \rangle$.

Mesh	NoCells	$\Delta_{x,min}$ [mm]	$\Delta_{x,max}$ [mm]	$\Delta_{x,st}$ [mm]
NU1	127,658	0.1	0.23	0.13
NU2	33,300	0.2	0.45	0.24
NU3	9225	0.4	0.82	0.45

The fuel jet and the air coflow enter the domain at a temperature of 300 K. The mixture fraction varies between $Z = 1$ at the jet and $Z = 0$ at the coflow, while $c = 0$ in both streams. For the outflow p employs a total pressure boundary condition, while zero normal gradient is set for the remaining flow variables. The boundary conditions to solve the system described by Equations (7)–(10) are summarized in Table 2.

Table 2. Boundary conditions. z.G. stands for zero normal gradient.

	Z	c	u [m/s]	p [Pa]
Jet	1	0	parabolic profile, u_{max}0.23	z.G.
Coflow	0	0	0.23	z.G.
Side wall	0	0	no-slip	z.G.
Outflow	z.G.	z.G.	z.G.	101,325

2.6. Filtered Chemical Database

The manifold is generated using the FGM method with planar steady counterflow diffusion flamelets. The set of Equations (1)–(5) are solved for a strain rate ranging from 0.03 s^{-1}, which can be considered as chemical equilibrium, up to 482 s^{-1}, after which extinction takes place. In order to fully span the composition space, unsteady flamelets are employed. The last ignited flamelet is taken as initial condition, the strain rate is increased, and time-dependent flamelet solutions are computed until the pure mixing condition is reached.

The flamelets have been generated employing the detailed chemistry solver CHEM1D [37], where the $GRI-3.0$ [38] detailed chemical mechanism has been considered with $Le = 1$ assumption. This mechanism has been developed to simulate natural gas mixtures, it is characterized by a comprehensive range of validated applicability, and for its low tendency to run into stiffness problems [1]. For this reason it has been widely employed, a non exhaustive list of applications includes the CH_4-Air chemical database generation for a novel coupled Principal Components Analysis (PCA)-LES model [39], NO_x prediction [40], cryogenic CH_4-O_2 flames [41], auto-ignition of CH_4 in hot vitiated coflow [42], and biomass-derived syngas modeling [43]. The progress variable is computed according to Equation (6), the selected species i are CO_2, H_2O and H_2, and the weight factor $\gamma_i^* = 1/MW_i$ is the inverse of the molecular weight as proposed in [33], though highly promising techniques such as PCA [44] might as well offer appealing alternatives to be appraised in future studies.

The flamelet solutions are filtered employing the Gaussian filter operator from Equation (13). Additional to the thermochemical quantities and the closure terms, the look-up table contains a flamelet label K_{Label}. It is defined as the strain rate at the

oxidizer side of the unfiltered solution, and indicates the flamelet from which each filtered profile has been obtained.

3. Results

This section presents the solution of the laminar coflow diffusion flame introduced above, applying the non-premixed filtered tabulated chemistry formulation. First, non-satisfactory results are obtained and the reasons for the observed deviations are discussed. A model activation strategy employing a sensor S based on the flame dimensionality is proposed. The performance of the non-premixed filtered tabulated chemistry formulation coupled with the novel flame sensor is assessed, and good agreement with the reference solution is achieved.

3.1. Filtered Tabulated Chemistry Problem

The case was solved applying the non-premixed filtered tabulated chemistry formulation. This procedure was carried out for three different filter sizes: $\Delta = 2, 3, 4$ mm. For all of the cases an unphysical mixture fraction evolution, which worsened with increasing filter size, was obtained. The results corresponding to $\Delta = 2$ mm are shown in Figure 2 where an already evident deviation from the reference can be seen, while not all the trends of the original solution have been lost.

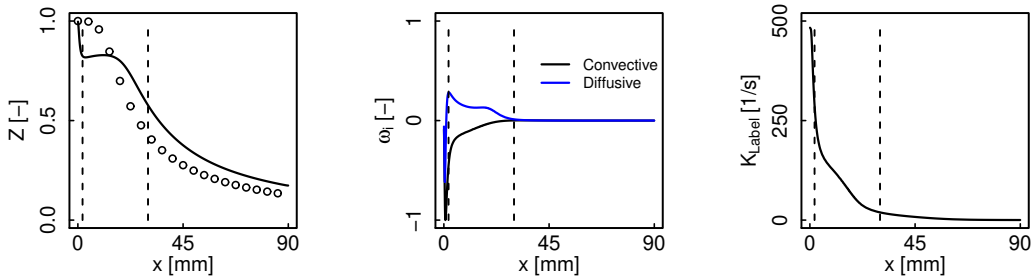

(**a**) Mixture fraction (**b**) Z source terms (**c**) Flamelet label

Figure 2. Centerline profiles of mixture fraction, normalized model correction terms and strain rate for $\Delta = 2$ mm. Solid lines represent the filtered tabulated chemistry results, circles correspond to the reference solution. The convention [–] is employed to denote non-dimensional quantities.

The reason for Z distortion relies on the model correction terms from Equation (9), whose behavior is shown in Figure 2b. Initially both of the terms are negative and reach their highest value close to the inlet, resulting in a steep Z decay. The subsequent sign change of the diffusive term is responsible for the inflection point on the Z profile starting from the first dashed line. The summation of the correction terms becomes positive, causing an unphysical Z increase, and then it balances. No trend difference with respect to the reference solution can be appreciated on the Z profile in the vicinity of the second dashed line, which indicates the point where the correction terms finally vanish.

This uneven model contribution results from the varying filter effect throughout the manifold. Figure 2c presents the behavior of the flamelet label, which associates a point in the filtered manifold to the unfiltered flamelet from which this value was derived. The profile coincides with previous studies which recall a strong scalar dissipation rate decay along the jet axis, as the distance from the nozzle increases [45,46]. The higher strained flamelets possess a lower thickness, they are more sensitive to the filter operation and for this reason high correction values on Figure 2b coincide with elevated K_{Label} on Figure 2c.

Filtered Manifold Transformation

Aiming to further depict the filter effect as a function of the flamelet strain rate, Figure 3 shows the profile transformation undergone by the two extreme steady flamelets of the current manifold, i.e., the equilibrium and the last ignited flamelets, under three different filter sizes. The equilibrium flamelet has a large thickness and it is essentially

not affected by the filtering operation so that the three profiles overlap becoming indistinguishable. This behavior categorically changes for $K = 482\ s^{-1}$, that completely changes its shape for each filter size. For instance using $\Delta = 5$ mm the progress variable profile loses its peak close to Z_{st} and instead it is centered at $Z = 0.5$, from where it is symmetrically distributed over the domain.

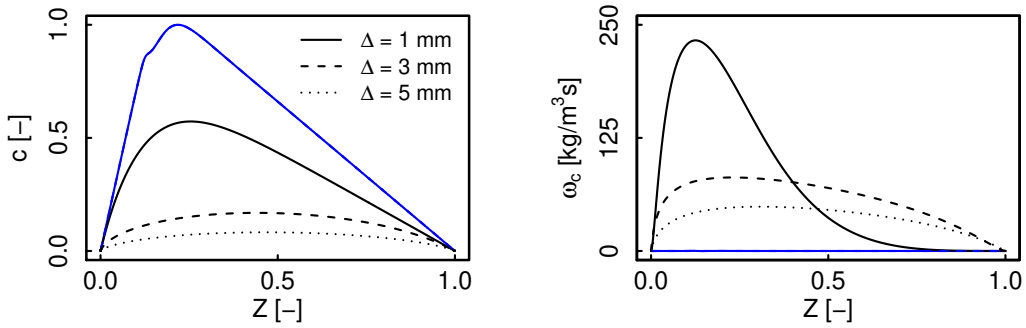

(**a**) Progress variable (**b**) c chemical source term

Figure 3. Flamelet transformation for two different strain rates and three filter sizes. Blue lines $K = 0.03\ s^{-1}$ and black lines $K = 482\ s^{-1}$. The three blue lines superimpose so that only one profile can be perceived.

The source term increases with K, so that for these extreme flamelets $\dot{\omega}_c$ does not even share the order of magnitude. For instance at $K = 482\ s^{-1}$ and $\Delta = 3$ mm, $\dot{\omega}_c$ extends all over the domain and the reactive zone can no longer be individualized. Deviations between the approximated and resolved diffusive and convective transport terms arise for the last ignited flamelet, while the equilibrium flamelet is not modified by the filtering operation, and consequently the correction terms are zero. This feature, namely the high filter sensitivity of the last ignited flamelet opposed to the unaltered equilibrium flamelet behavior explains the disappearance of the correction terms after the second dashed line in Figure 2b, as K goes beneath a low threshold value.

When assembling a manifold of counterflow flamelets, c decreases with K for any given Z, except for the extremes where all the profiles converge. On a real coflow flame the fuel side might considerably distinguish from the counterflow setup due to geometrical constraints and flow orientation. In such a situation, c evolution in the actual flame describes a K profile that departs from a high value at the fuel side and that subsequently decreases towards c_{max} location, where the flame structure resembles the counterflow configuration. This is the case at the centerline, so the obtained profile is coherent with the manifold intrinsic features, and the observed Z deviations obtained with the filtered tabulated chemistry approach result from the substantial role of the flamelet strain in the model performance. These outcomes, namely the flamelet strain rate filter sensitivity and the manifold-conditioned centerline strain rate profile do not only elucidate the results exhibited in Figure 2, but moreover point out the need of an additional tool to determine the use of the model correction terms.

3.2. Flame Sensor

A flame sensor can be employed on filtered or thickened flame front approaches to control the model activation and thus distinguish between reacting and pure mixing (non reacting) zones, e.g., based on c [47]

$$S = 16[c(1-c)]^2, \tag{16}$$

on its source term $\dot{\omega}_c$[48]

$$S = max\left[\frac{tanh\left(100\frac{\widetilde{\dot{\omega}}_c(\tilde{c},\tilde{Z})}{\widetilde{\dot{\omega}}_{c,max}(\tilde{Z})} - 0.25\right)}{0.75}; 0\right], \tag{17}$$

or on its gradient [49]

$$S = \left[\frac{\frac{\partial c}{\partial x}}{max\left(\frac{\partial c}{\partial x}\right)}\right]_{1-D}, \tag{18}$$

where $1 - D$ indicates that both of the values are read from the detailed chemistry flamelets. Hence S is computed on the fly for Equation (16), whilst $S = f(Z, c)$ is precomputed and stored in the lookup table for Equations (17) and (18). For the deactivated sensor condition, the scalar transport is fully determined by convection and diffusion which can be adequately resolved on the numerical grid. A sensor based on the mixture fraction gradient is proposed in order to guarantee the counterflow flame hypothesis and thus the appropriate performance of the non-premixed filtered tabulated chemistry model.

3.2.1. Justification

The one-dimensional counterflow configuration assumption is a key issue in the derivation of the non-premixed filtered tabulated chemistry model. This constraint does not rely on the filtering principle itself, which can be applied to any arbitrary configuration, but it is due to the fact that the model correction terms have been determined as to satisfy the equations describing this specific configuration. Nonetheless, there are phenomena taking place on multidimensional non premixed laminar flames which do not coincide with the fundamental flamelet assumptions, as has already been pointed out by several authors [50]. The one dimensional hypothesis correctly describes an idealized planar counterflow flame, but for a coflow flame the consideration of multidimensional effects results imperative. For instance, it has been shown that under given simplifications, e.g., radiation and differential diffusion being neglected, steady flamelets adequately recover the main flame features, while discrepancies are observed principally along the centerline [51].

An exhaustive comparison between detailed chemistry and FGM results for the current study case is presented in [33]. The authors show that when the assumption $Le = 1$ is employed, even though FGM and detailed chemistry results coincide, tangential diffusion and curvature effects play a significant role at the centerline. Their repercussion becomes detectable as soon as the diffusion coefficient is distinctively calculated for each species, and FGM results deviate from the detailed chemistry ones.

In order to illustrate the multidimensional effects, Figure 4 presents the mixture fraction and species gradient orientation, defined as

$$\theta_{\nabla\varphi} = tan^{-1}\left(\frac{\nabla\varphi_x}{max\left(|\nabla\varphi_y|, tol\right)}\right) \tag{19}$$

where tol is a tolerance to avoid dividing by zero for a non-monotonic φ evolution. $\theta_{\nabla\varphi} = 0$ corresponds to the one dimensional counterflow flame hypothesis, while $\theta_{\nabla\varphi} = \pm 90$ describes a gradient evolving along the axial direction. The case has been solved employing the detailed chemistry solver laminarSimpleSMOKE [52–54] with unitary Lewis number assumption.

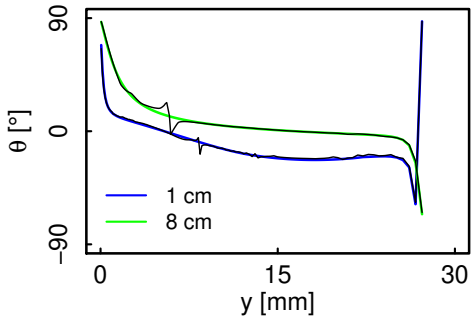

Figure 4. Gradient angle profiles at two different radial sections. Colored lines correspond to ∇Z , black lines are ∇CO_2.

The radial gradient dominates and the angle tends to 0° in the majority of the domain. Nevertheless, a deviation from this behavior is obtained at the extremes, i.e., close to the centerline and at the side, where $\theta_{\nabla Z} \approx 90°$. The results presented in Section 3.1 showed big model deviations at the centerline, precisely where Figure 4 highlights the presence of multidimensional phenomena, which is indeed reasonable given that the model falls out of scope. In this way, an approach is proposed which assesses the model performance by activating the correction terms exclusively in the counterflow regions, taking advantage of a sensor based on ∇Z.

This formulation has been chosen exploiting the fact that the flamelet thickness decreases with the strain rate, consequently modifying the gradients. Based on one-dimensional flamelet characterizing features two assumptions are made, whose adequacy will be appraised afterwards. Defining a point P described by the pair (Z_P, c_P), the first hypothesis states the uniqueness of the mixture fraction gradient, i.e., non-coincidence for different configurations. Second, it is assumed that the maximum possible gradient will be obtained on a counterflow condition. In other words, if P does not comply with a counterflow condition, the flame front will unquestionably possess a lower strain rate than the counterflow flamelet corresponding with these coordinates.

3.2.2. Proposed Definition

Considering that on a flamelet-based approach the flame front can be visualized as a set of thin mixture fraction iso-surfaces [21,28], it follows that for every single point, the gradient of the transported mixture fraction ∇Z_{sim} should coincide with that of the accessed flamelet ∇Z_{fl}. The underlying assumption being that both the flamelet and the real flame front share the same resolution, which in general is not the case, and as a matter of fact is the motivation for the filtered tabulated chemistry model.

The flamelet solution has been computed with CHEM1D [37], which utilizes an adaptive gridding strategy where a mesh function depending on the gradient and curvature of all variables optimizes the position of the grid points [37]. For a Gaussian filter, the numerical grid resolution, i.e., the amount of nodes defined within a given filter size affects the quality of the discrete approximation [14]. Therefore, before performing the filtering operation the flamelet is reinterpolated over a new mesh, each cell size being the minimum between the original cell size and $\Delta/5$, as suggested in [22]. This is necessary in order to adequately compute the correction terms and for the reconstruction of the retrieved variables $\Phi = f(Z, c)$. However this has deep consequences in ∇Z computation when compared to a lower resolution mesh. To illustrate this, Figure 5 compares the normalized mixture fraction gradient behavior of two strained flamelets when varying the numerical grid resolution. First each flamelet was directly filtered with $\Delta = 2$ mm and ∇Z was computed. Three different Δ/Δ_x ratios were defined and constantly spaced progressions mimicking coarser numerical grids were generated. The filtered flamelet Z profile was projected over these new domains and ∇Z were subsequently computed employing finite differences.

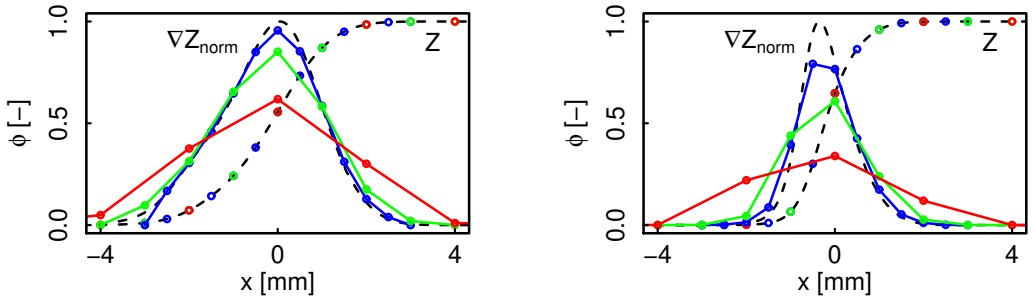

(**a**) $K = 100\ \mathrm{s}^{-1}$ (**b**) $K = 500\ \mathrm{s}^{-1}$

Figure 5. Numerical grid resolution effect over the mixture fraction gradient for two CH_4-*Air* flamelets with $\Delta = 2$ mm. Blue line $\Delta/\Delta_x = 4$, green line $\Delta/\Delta_x = 2$, red line $\Delta/\Delta_x = 1$, dashed lines are the reference filtered flamelet.

Given that the domain is described with less points, as the ratio Δ/Δ_x decreases so does the resolution in the reactive zone. This effect becomes more perceivable as K increases, due to the already mentioned thickness variation along a non-premixed manifold. For instance $\Delta/\Delta_x = 2$ reproduces quite well ∇Z profile for $K = 100\ \mathrm{s}^{-1}$, while a considerable deviation is observed for $K = 500\ \mathrm{s}^{-1}$, and this discrepancy will vary depending on the specific point around which the gradient is computed. An analogous behavior has been reported on filtered premixed flames, where the minimum number of points to capture the filtered flame front and correctly retrieve the flame speed have been assessed considering the filtered thermal flame thickness $\delta_{\tilde{c}} = 1/max\left(\frac{\partial \tilde{c}}{\partial x}\right)$ [22] and the filtered reaction zone thickness $\overline{\delta}_r$, defined as the full width at half maximum of the reaction rate $\dot{\omega}_c$ [23,55]. Based on these considerations a flame sensor S comparing the simulation and reference flamelet mixture fraction gradients is proposed as

$$S = H(\nabla Z_{sim}/\nabla Z_{fl} - ct) = \begin{cases} 0 & \text{if} \quad \nabla Z_{sim}/\nabla Z_{fl} < ct \\ 1 & \text{if} \quad \nabla Z_{sim}/\nabla Z_{fl} \geq ct \end{cases}, \tag{20}$$

where H is the Heaviside or unit step function and ct corresponds to a tolerance that takes into account the varying effect of the numerical grid resolution along K. The transport equation for the parametrizing variables finally reads

$$\frac{\partial \bar{\rho}\tilde{\varphi}}{\partial t} + \nabla \cdot (\bar{\rho}\tilde{u}\tilde{\varphi}) = \nabla \cdot (\bar{D}\nabla\tilde{\varphi}) + \overline{\dot{\omega}}_{\varphi} + S\left(\Omega_{\varphi} + \alpha_{\varphi}\right). \tag{21}$$

3.3. Filtered Tabulated Chemistry Results

The reference solution was obtained following the procedure suggested in [33] employing a FGM manifold. The chemical database was constructed as explained in Section 2.6, the difference with respect to the non-premixed filtered tabulated chemistry manifold being that the filtering operation was omitted. The parameterizing variables transport equations were solved together with the continuity and momentum equations. These equations distinguish themselves from Equations (7)–(10) that no filtering operation was applied either. Apart from the chemical database and the transport equations, all the other case features, i.e., the computational grid, boundary conditions and numerical settings remained unmodified. The results satisfactorily coincided with those in [33]. The choice of this reference solution ensures that any difference with respect to the filtered tabulated chemistry approach must rely on the filtering operation. This is not the case for instance if the detailed chemistry solution with $Le = 1$ is employed, where the filtering transformation and possible differences due to the steady counterflow flamelets cannot be decoupled.

The case was now solved applying the novel flame sensor with $ct = 0.9$ within the non-premixed filtered tabulated chemistry formulation as in Section 2.2. For the current laminar case this transformation, and the use of filtered tables is equivalent to perform a filtering operation over the whole domain. Exploiting this quite convenient feature, the results could be compared against the ones obtained applying a Gaussian filter to the reference solution. This procedure was carried out for three different filter sizes: $\Delta = 2, 3, 4$ mm.

For each filter size, simulations were carried out using three numerical grids in order to assess the influence of the numerical mesh resolution over the results. For the smaller filter size, i.e., $\Delta = 2$ mm, this corresponds to a ratio between the filter size and the grid spacing $\Delta/\Delta_x = 20, 10$ and 5. Good agreement is obtained between the three numerical grids, which is in accordance with the previous findings of Coussement [27], where a ratio $\Delta/\Delta_x = 5$ proved to adequately resolve the flame front. The results match correctly the reference data as can be observed in Figure 6.

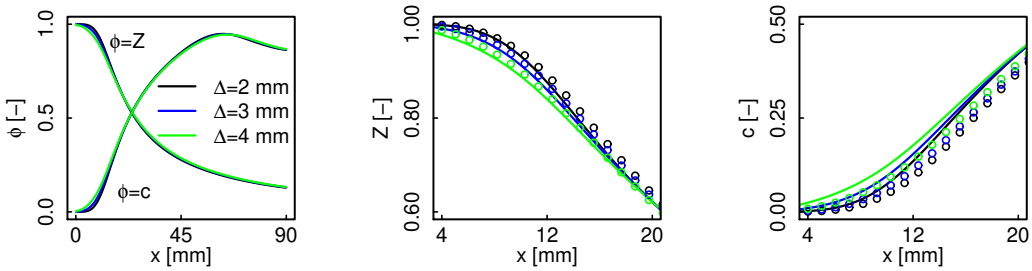

(**a**) Z and c axial profiles (**b**) Zoomed Z (**c**) Zoomed c

Figure 6. Filtered axial profiles of mixture fraction and progress variable (**a**); zoom of region with bigger filter effect for Z (**b**) and for c (**c**). Solid lines represent the filtered tabulated chemistry results, circles correspond to the filtered reference solution.

The ignition zone, which corresponds to the region with the biggest gradients along the centerline has been zoomed in Figure 6b,c. It can be observed that the model is able to adequately retrieve the profile transformation resulting from the filtering process. The mixture fraction decay is over predicted with a maximum relative error $RE_Z = 5.1\%$, corresponding to $\Delta = 4$ mm. From the physical point of view this variation entrains a decrease in the unignited flame core which is shifted backwards and induces the displacement of c profile.

The radial profiles accurately match the filtered reference solution. Following the small mixture fraction gradients in the radial direction, modest differences, not surpassing an absolute error of $AE_Z = 0.02$ are found at $x = 1$ cm, while downstream the profile change is almost negligible as shown in the left column of Figure 7. Non-monotonically evolving functions undergo a substantially bigger profile transformation in which the peak values decrease as a function of the species profile thickness. Excellent agreement is obtained for OH profiles, where the peak value is predicted with a maximum $RE_{OH} = 6.7\%$, which occurs at $x = 8$ cm and $\Delta = 4$ mm. The progress variable is satisfactorily described as well, though the profile shows lower sensitivity to the filtering process as a result of its higher thickness.

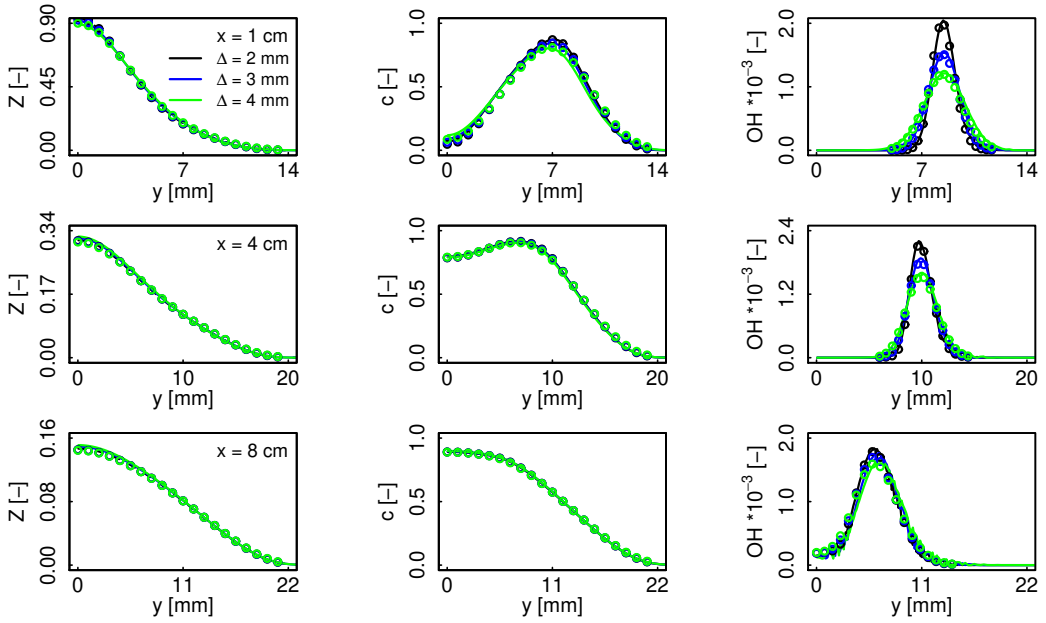

Figure 7. Filtered radial profiles. Solid lines represent the filtered tabulated chemistry results, circles correspond to the filtered reference solution.

4. Discussion

The coupling of the non-premixed filtered tabulated chemistry and the flame sensor delivered satisfactory results by ensuring the model activation based on the fulfillment of the counterflow flame hypothesis. This section expands the model understanding considering three aspects: the existence of conserved features in the filtered flame structure, the relevance of the model correction terms, and the sensor response throughout the domain.

4.1. Flame Structure

The Z centerline profile decay and the radial expansion cause the mixture fraction gradients to decrease downstream, i.e., a less strained flame front. It follows that a given filter size might produce considerable modifications at a given location, and be rather negligible on a further downstream section. For instance, while at $x = 1$ cm both c and OH are modified, c appears to remain unaltered at $x = 4$ cm, and at $x = 8$ cm there is a minor filter effect even for OH. This filter sensitivity variation along the domain represents the biggest challenge when applying the non-premixed filtered tabulated chemistry model on a real diffusive laminar flame. The strain variations along iso-Z surfaces result into flamelet interactions [21], and an adequate filtered flame structure prediction must take this feature into account considering modified and unmodified flamelets.

Figure 8 presents K_{Label} behavior, which is a tag relating every point in the filtered manifold to the unfiltered flamelet from which it was derived. Defining Z_C as the highest value for which K_{Label} coincides for all the filter sizes, the filtered flame structure is divided into two regions in Z space. The first covers the range $Z < Z_C$, within which c profiles might differ, and the second region comprises $Z > Z_C$ where c profiles converge despite distinct K_{Label} values. It is known that one-dimensional flamelets in general terms can adequately describe a diffusion flame, and that difficulties emerge close to the centerline due to multidimensional effects [51]. However, the first region indicates that far from the centerline, there is a zone whose flame structure can be described as the filtering of the same $Z - c$ trajectory. This is a quite encouraging result, as it suggests the existence of a conserved flame feature which can be recovered throughout the filtering of counterflow flamelets.

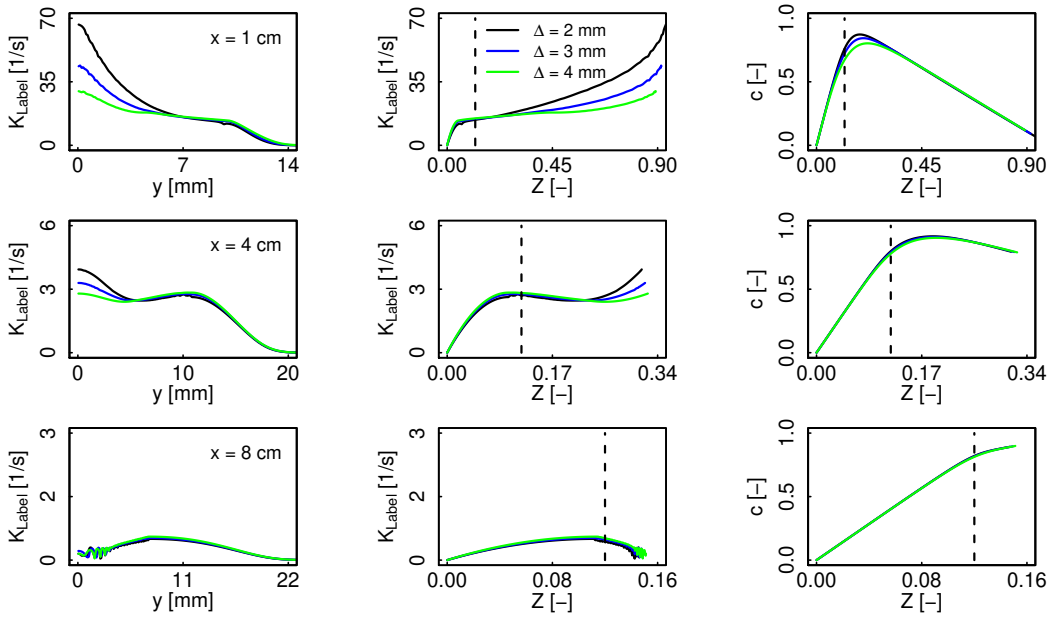

Figure 8. Strain rate and progress variable radial profiles in physical and mixture fraction space. Solid lines radial profiles, vertical dashed line Z_{st}.

Close to the centerline, on the contrary, the counterflow hypothesis is not appropriate and K_{Label} decreases with the filter size. The good agreement with the filtered reference solution highlights the non-premixed filtered tabulated chemistry capability to describe the filtered flame structure, even though the formulation cannot ensure the conservation of a flame feature for this particular region. The results suggest that including the correction terms for an active sensor, while no strategy is proposed for the deactivated condition, though being an apparently crude assumption, can appropriately depict the undergoing physics.

4.2. Model Correction Terms Sensitivity

In order to evaluate the role of the model itself, the case was resolved employing filtered tables but deactivating the correction terms. Figure 9a shows that along the centerline the use of different filter sizes without additional correction terms does not exert any change neither on Z nor on c profiles, and they converge to the original unfiltered values. The same behavior is appreciated as well for radial Z profiles, which remain unaltered in Figure 9b. These results outline the model correction terms relevance in order to retrieve the correct profile expansion, analogous to the flame front propagation speed under prediction reported in the premixed filtered tabulated chemistry approach when neglecting the model contribution [22]. Figure 9c shows that the decrease in peak values, on the contrary, is mostly dominated by the filtering operation and not by the addition of correction terms. This can occur in two ways: for a transported variable, e.g., c, this is the effect of a lessened $\dot{\omega}_c$ as a result of the filtering operation; while for the tabulated values, i.e., $\Phi = f(Z, c)$, the profile modification will take place as a simultaneous effect of decreased c and of the modified Φ profiles themselves.

4.3. Sensor Performance

The sensor tolerance is bounded between two conditions: $ct_{Max} \leq ct \leq 1$ where S is permanently deactivated, and $0 < ct \leq ct_{Min}$ where it is always active. In order to assure the activation flexibility and simultaneously guarantee the correctness of the results, a sensitivity analysis was carried out, and the optimal ct value was defined as the minimum for which two successive ct curves converged. Figure 10 depicts the model response for the three different filter sizes from where the tolerance was determined as $ct = 0.9$, as it coincides with $ct = 0.95$ for all the filter sizes. The model sensitivity increases with the filter

size, thus while $ct = 0.9$ and $ct = 0.8$ profiles converge for $\Delta = 2$ mm, a slight deviation is observed for $\Delta = 3$ mm and they are clearly distinguishable for $\Delta = 4$ mm. In order to further illustrate ct relevance, the three dashed lines evidence the increasing model distortion that results from decreasing tolerance values.

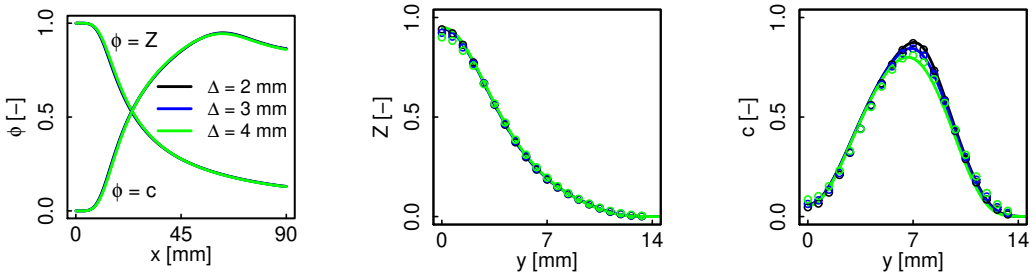

(**a**) Z and c at centerline (**b**) Z at x = 1 cm (**c**) c at x = 1 cm

Figure 9. Mixture fraction and progress variable centerline and radial profiles for three different filter sizes. The manifolds are generated by direct flamelet filtering, the filtered tabulated chemistry correction terms being omitted.

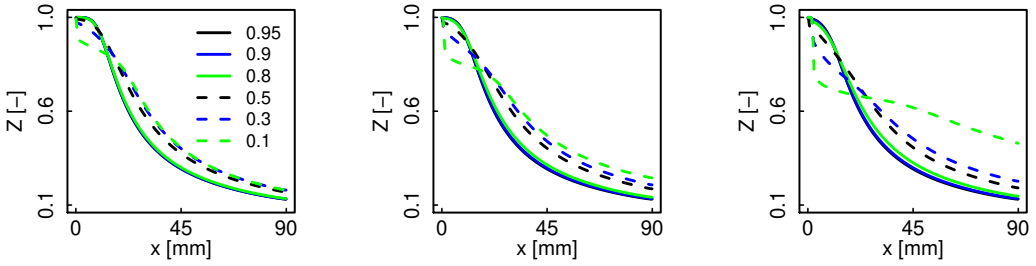

(**a**) $\Delta = 2$ mm (**b**) $\Delta = 3$ mm (**c**) $\Delta = 4$ mm

Figure 10. Effect of ct variation, assessed on the Z centerline profiles for three different filter sizes.

Figure 11 shows the appropriate sensor response throughout the reaction zone, in compliance with the one-dimensional behavior recalled on Figure 8. Though both Equation (18) and the proposed sensor definition in Equation (20) are based on the gradient of a parameterizing scalar, there is a substantial conceptual distinction. The former compares ∇c with its maximum value for a given equivalence ratio, thus it covers the entire c profile [49], and its response is exclusively determined by the precomputed flamelet's topology to ensure the appropriate flame front expansion. The current S compares the resolved ∇Z with the tabulated one, thus additional to Z and c, it is a function of the numerical configuration as well. The response of the proposed sensor is not a-priori constrained to a specific region in chemical space, but on the contrary it will depend on the specific conditions at every flame point. Close to the centerline the gradients in the axial direction play a non-negligible role and the one-dimensional flamelet hypothesis loses its validity [50], resulting into S radial offset. Furthermore, the varying mixture fraction top limit observed in Figure 11a appears to be an essential feature, hence highlighting the unsuitableness of a sensor formulation permanently acting in the vicinity of the flame [47], i.e., based on fixed composition space zones. The sensor adequately responds to the flame thickening caused by the strain rate decrease downstream as S active range expands in order to fully encompass the lean region of the flame.

Due to the increasing filter sensitivity with the strain rate, i.e., a more significant flamelet transformation, an arbitrary manifold region occupied by temporary evolving flamelets, might be replaced by their steady counterparts after the filtering operation. Hence, the characterization of the flame lift-off zone depicts a particularly challenging condition for the non-premixed filtered tabulated chemistry formalism. Given that it is not straightforward to theoretically sustain the sensor adequacy under this condition, an interpretation rather than a justification of the sensor performance is presented.

Figures 12 and 13 depict two filtered steady flamelets whose profiles lie over unfiltered unsteady profiles when observed in mixture fraction space.

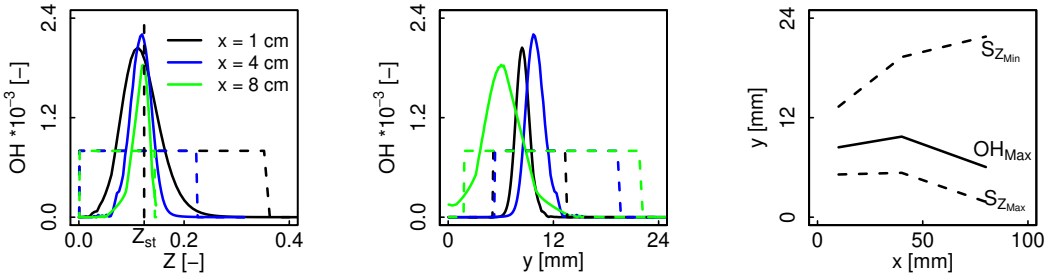

(**a**) (**b**) (**c**)

Figure 11. OH radial profiles for $\Delta = 2$ mm at different downstream locations represented in mixture fraction (**a**) and physical space (**b**). (**c**) corresponds to the limit values of (**b**) along the axial direction. Solid lines OH, dashed lines flame sensor.

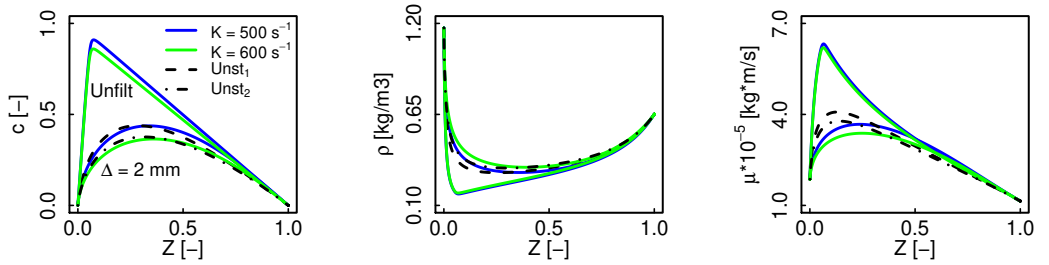

(**a**) Progress variable (**b**) Density (**c**) Viscosity

Figure 12. Variable transformation due to filtering for two steady state flamelets and their similitude with unfiltered unsteady flamelets when plotted in Z space. Solid lines steady profiles, dashed lines unsteady profiles.

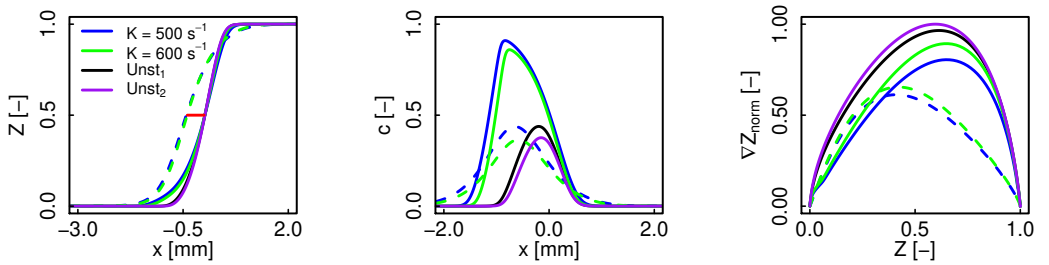

(**a**) (**b**) (**c**)

Figure 13. Profile distinction for Z space analogous trajectories of steady filtered and unsteady unfiltered flamelets when observed in the physical space. Solid lines unfiltered profiles, dashed lines filtered profiles, and the red line is a separation included to better individualize the curves.

The first aspect that calls the attention is that even though the variables behavior in Figure 12 shows a considerably good accordance between the unsteady and the filtered steady flamelets projected in Z space, their physical space profiles significantly differ as shown in Figure 13a. Since the manifold expansion beyond the last ignited flamelet is done is by simulating an unsteady extinguishing flamelet that is subsequently used as a natural continuation of the manifold [56], the unsteady flamelets tend to keep the same domain length as their originating flamelet, while the filtered ones will expand respect to their unfiltered counterpart. As a result of this for the same $Z - c$ combination the ∇Z profiles are considerably lower for the filtered flamelets than for the unsteady ones. The corollary is that in order for the filtered steady flamelets to perform a continuation role,

∇Z_{sim} should be smaller than that of the accessed flamelet, and consequently it will be significantly smaller than the original unsteady counterpart. Otherwise, the point describes a steady filtered flamelet, with the corresponding model correction terms. Being aware that continuation methods to fully span the chemical space might introduce some non-smoothness in the non-premixed manifold [57], the correct flame location confirms that the initial, non-ignited region can be adequately described employing filtered flamelets, acknowledging the adequate deactivated sensor response.

Expanding on this aspect, the sensor can be more globally interpreted as a flamelet identifier. In this way, independent of the location in Z space, an active sensor describes a point which behaves as a counterflow filtered flamelet, while the contrary corresponds to a point that obeys the variable transport while not fulfilling the model hypothesis. For instance, analogous to premixed flames were the flame sensor should ensure an accurate computation of pure mixing, i.e., constant progress variable regions [58], another condition under which the proposed flame sensor results useful are the constant mixture fraction regions. This might happen at the domain extremes, e.g., at the fuel core, but might as well take place inside the Z domain, e.g., piloted flames such as Sandia flame series, in which the composition of the pilot stream is projected onto a single mixture fraction [59]. In any of the cases the constant valued Z zone imposes a particular constraint within the system, so that the addition of the model correction terms would deliver unphysical results. The sensor appropriately handles this situation, since ∇Z tends to zero, and consequently the model deactivation is assured.

5. Conclusions

The present work assessed the capability of the non-premixed filtered tabulated chemistry formalism to adequately describe the filtered flame structure of a real laminar coflow diffusion flame. The model appeared to be considerably sensitive to the flame dimensionality. Unphysical profile distortions arised when points described by highly strained regions of the manifold, and consequently having big model correction terms, did not comply with the one-dimensional flamelet hypothesis. Aiming to verify the soundness of this assumption a flame sensor based on the mixture fraction gradient, with a tolerance to take into account the numerical grid resolution, was introduced.

Simulations performed using the model coupled with the flame sensor were compared against the direct filtering of a reference solution, and good agreement was obtained for the laminar flame. This is a fundamental result as it demonstrates the capability of the formalism to preserve the flame characteristic features. In this way the sensor determined model activation adequately represents the underlying physics behind flame filtering and so it endorses the consistency of the numerical procedure.

Expanding on the findings, using three different filter sizes, it turned out that:

- Far from the centerline the flame front does not only satisfy the counterflow hypothesis, but the flamelet identifier K_{Label} remains unaltered after the filtering operation, what can be understood as the filtering of the same trajectory, namely of the same flamelet.
- The effect of a modified filtered profile at the reaction zone is then transported through convection and diffusion towards higher Z zones, and is the cause for the centerline profile modifications, where the model is not active.
- The profile extension due to the filtering process is mainly driven by the model correction terms, while the decrease in the peak values of non monotonically evolving variables depends on the filtered parameters that enter the transport equation.
- The sensor adequately identifies the multidimensional effect at the centerline, and its active range both in Z as in physical space changes throughout the domain, in accordance with the strain rate decrease and higher flame thickness.

The flame thickness within a non-premixed counterflow flamelets manifold spans several orders of magnitude as function of K. Due to the random nature of eddies, the strain rate oscillates within a range in turbulent flames, therefore flame front resolution can generally not be ensured for the whole spectrum of possible values. Though flame front filtering appears as a natural alternative to relax the resolution constraint, the capability of such an approach had so far been questioned due to the difficulty in the definition of a conserved property. This study unambiguously proves that it is possible to adequately capture the filtered structure of a real diffusion flame and conserve the flame characteristic features. This is a quite relevant issue for the combustion community, for the method opens a new spectrum of possibilities for the development of closure strategies based on an explicit coupling between the step size of the computational grid and a non-premixed flamelets database. Hence, the present study sets a milestone towards the application of non-premixed filtered tabulated chemistry as a turbulent combustion modeling strategy in the LES framework. The promising results obtained on the coflow laminar diffusion flame encourage the further model appraisal on a more complex turbulent configuration. The following work will not only pursue the assessment of the model and flame sensor performances in turbulent combustion, but it will as well propose an strategy to take into account the modified turbulence-chemistry interaction due to the filtering operation.

Supplementary Materials: The following are available at www.mdpi.com/xxx/s1. Laminar flame unfiltered and filtered data.

Author Contributions: Conceptualization, P.J.O.V. and A.C.; methodology, P.J.O.V. and A.C.; software, P.J.O.V.; validation, P.J.O.V.; investigation, P.J.O.V.; writing—original draft preparation, P.J.O.V.; writing—review and editing, A.C., A.S. and A.P.; supervision, A.C., A.S. and A.P.; project administration, A.S. and A.P.; funding acquisition, A.S. and A.P. All authors have read and agreed to the published version of the manuscript.

Funding: This work has received funding from the European Union's Horizon 2020 research and innovation program under the Marie Sklodowska- Curie grant agreement No 643134. This work has also received funding from the European Research Council, Starting Grant No. 714605. Calculations for this research were conducted on the Lichtenberg high performance computer of the TU Darmstadt.

Institutional Review Board Statement: Not applicable.

Informed Consent Statement: Not applicable.

Data Availability Statement: The data presented in this study are available as Supplementary Materials.

Conflicts of Interest: The authors declare no conflict of interest. The funders had no role in the design of the study; in the collection, analyses, or interpretation of data; in the writing of the manuscript, or in the decision to publish the results.

Nomenclature

Greek letters

α_φ	Unresolved diffusive contribution
γ_i	Progress variable species i weight factor
δ	Flame thickness
λ	Thermal conductivity
φ	Specific value of a parameterizing variable
ρ	Mass density
τ	Laminar viscous tensor
$\dot{\omega}$	Chemical production rate
Δ	Filter size
Δ_x	Numerical grid spacing
Ω_φ	Unresolved convective contribution

Latin letters

c	Progress variable
c_p	Specific heat at constant pressure
h	Enthalpy
p	Pressure
s	Spatial coordinate perpendicular to the flame front
u	Velocity
D	Molecular diffusivity
K	Strain rate
K_{Label}	Flamelet label
Le	Lewis number
S	Flame sensor
Y_i	Mass fraction of species i
Z	Mixture fraction

References

1. Curran, H.J. Developing detailed chemical kinetic mechanisms for fuel combustion. *Proc. Combust. Inst.* **2019**, *37*, 57–81. [CrossRef]
2. Van Oijen, J.; Donini, A.; Bastiaans, R.; ten Thije Boonkkamp, J.; De Goey, L. State-of-the-art in premixed combustion modeling using flamelet generated manifolds. *Prog. Energy Combust. Sci.* **2016**, *57*, 30–74. [CrossRef]
3. van Oijen, J.A. *Flamelet-Generated Manifolds: Development and Application To Premixed Laminar Flames*; Technische Universiteit Eindhoven Eindhoven: Eindhoven, The Netherlands, 2002.
4. Gicquel, O.; Darabiha, N.; Thévenin, D. Liminar premixed hydrogen/air counterflow flame simulations using flame prolongation of ILDM with differential diffusion. *Proc. Combust. Inst.* **2000**, *28*, 1901–1908. [CrossRef]
5. Pierce, C.D.; Moin, P. Progress-variable approach for large-eddy simulation of non-premixed turbulent combustion. *J. Fluid Mech.* **2004**, *504*, 73–97. [CrossRef]
6. Ihme, M.; Cha, C.M.; Pitsch, H. Prediction of local extinction and re-ignition effects in non-premixed turbulent combustion using a flamelet/progress variable approach. *Proc. Combust. Inst.* **2005**, *30*, 793–800. [CrossRef]
7. Sacomano Filho, F.L.; Hosseinzadeh, A.; Sadiki, A.; Janicka, J. On the interaction between turbulence and ethanol spray combustion using a dynamic wrinkling model coupled with tabulated chemistry. *Combust. Flame* **2020**, *215*, 203–220. [CrossRef]
8. Colin, O.; Ducros, F.; Veynante, D.; Poinsot, T. A thickened flame model for large eddy simulations of turbulent premixed combustion. *Phys. Fluids* **2000**, *12*, 1843–1863. [CrossRef]
9. Mahmoud, R.; Jangi, M.; Ries, F.; Fiorina, B.; Janicka, J.; Sadiki, A. Combustion Characteristics of a Non-Premixed Oxy-Flame Applying a Hybrid Filtered Eulerian Stochastic Field/Flamelet Progress Variable Approach. *Appl. Sci.* **2019**, *9*, 1320. [CrossRef]
10. Sarkar, S. Large Eddy Simulation of Flows of Engineering Interest: A Review. In *50 Years of CFD in Engineering Sciences*; Springer: Berlin/Heidelberg, Germany, 2020; pp. 363–400.
11. Poinsot, T.; Veynante, D. *Theoretical and Numerical Combustion*; R.T. Edwards Inc.: Montgomery, PA, USA, 2005.
12. Gicquel, L.Y.; Staffelbach, G.; Poinsot, T. Large eddy simulations of gaseous flames in gas turbine combustion chambers. *Prog. Energy Combust. Sci.* **2012**, *38*, 782–817. [CrossRef]
13. Luo, G.; Dai, H.; Dai, L.; Qian, Y.; Sha, C.; Zhang, Y.; Wu, B. Review on Large Eddy Simulation of Turbulent Premixed Combustion in Tubes. *J. Therm. Sci.* **2020**, *29*, 853–867. [CrossRef]
14. Pope, S.B. *Turbulent Flows*; Cambridge University Press: New York, NY, USA, 2001.
15. Sagaut, P. *Large Eddy Simulation for Incompressible Flows: An Introduction*; Springer Science & Business Media: New York, NY, USA, 2006.
16. Garnier, E.; Adams, N.; Sagaut, P. *Large Eddy Simulation for Compressible Flows*; Springer Science & Business Media: New York, NY, USA, 2009.
17. Pope, S.B. Ten questions concerning the large-eddy simulation of turbulent flows. *New J. Phys.* **2004**, *6*, 35. [CrossRef]
18. Celik, I.; Klein, M.; Janicka, J. Assessment measures for engineering LES applications. *J. Fluids Eng.* **2009**, *131*, 031102. [CrossRef]
19. Grigoriadis, D.G.; Geurts, B.J.; Kuerten, H.; Fröhlich, J.; Armenio, V. *Direct and Large-Eddy Simulation X*; Springer International Publishing: New York, NY, USA, 2018.
20. Salvetti, M.V.; Geurts, B.; Meyers, J.; Sagaut, P. *Quality and Reliability of Large-Eddy Simulations II*; Springer Science & Business Media: New York, NY, USA, 2010; Volume 16.
21. Veynante, D.; Vervisch, L. Turbulent combustion modeling. *Prog. Energy Combust. Sci.* **2002**, *28*, 193–266. [CrossRef]
22. Fiorina, B.; Vicquelin, R.; Auzillon, P.; Darabiha, N.; Gicquel, O.; Veynante, D. A filtered tabulated chemistry model for LES of premixed combustion. *Combust. Flame* **2010**, *157*, 465–475. [CrossRef]
23. Auzillon, P.; Gicquel, O.; Darabiha, N.; Veynante, D.; Fiorina, B. A filtered tabulated chemistry model for LES of stratified flames. *Combust. Flame* **2012**, *159*, 2704–2717. [CrossRef]

24. Mercier, R.; Auzillon, P.; Moureau, V.; Darabiha, N.; Gicquel, O.; Veynante, D.; Fiorina, B. Les modeling of the impact of heat losses and differential diffusion on turbulent stratified flame propagation: Application to the tu darmstadt stratified flame. *Flow Turbul. Combust.* **2014**, *93*, 349–381. [CrossRef]
25. Wang, L. Analysis of the filtered non-premixed turbulent flame. *Combust. Flame* **2017**, *175*, 259–269. [CrossRef]
26. Chan, W. A Higher-Order Flamelet Model for Turbulent Combustion Simulations. Ph.D. Thesis, University of Michigan, Ann Arbor, MI, USA, 2016.
27. Coussement, A.; Schmitt, T.; Fiorina, B. Filtered Tabulated Chemistry for non-premixed flames. *Proc. Combust. Inst.* **2015**, *35*, 1183–1190. [CrossRef]
28. Peters, N. *Turbulent Combustion*; Cambridge University Press: New York, NY, USA, 2001.
29. Donini, A.; Bastiaans, R.; van Oijen, J.; de Goey, L. A 5-D implementation of FGM for the large eddy simulation of a stratified swirled flame with heat loss in a gas turbine combustor. *Flow, Turbul. Combust.* **2017**, *98*, 887–922. [CrossRef] [PubMed]
30. De Goey, L.; ten Thije Boonkkamp, J. A flamelet description of premixed laminar flames and the relation with flame stretch. *Combust. Flame* **1999**, *119*, 253–271. [CrossRef]
31. De Goey, L.; ten Thije Boonkkamp, J. A mass-based definition of flame stretch for flames with finite thickness. *Combust. Sci. Technol.* **1997**, *122*, 399–405. [CrossRef]
32. Ramaekers, W.; Van Oijen, J.; De Goey, L. A priori testing of flamelet generated manifolds for turbulent partially premixed methane/air flames. *Flow, Turbul. Combust.* **2010**, *84*, 439–458. [CrossRef]
33. Verhoeven, L.; Ramaekers, W.; Van Oijen, J.; De Goey, L. Modeling non-premixed laminar co-flow flames using flamelet-generated manifolds. *Combust. Flame* **2012**, *159*, 230–241. [CrossRef]
34. Ries, F.; Obando, P.; Shevchuck, I.; Janicka, J.; Sadiki, A. Numerical analysis of turbulent flow dynamics and heat transport in a round jet at supercritical conditions. *Int. J. Heat Fluid Flow* **2017**, *66*, 172–184.
35. Caretto, L.; Gosman, A.; Patankar, S.; Spalding, D. Two calculation procedures for steady, three-dimensional flows with recirculation. In Proceedings of the Third International Conference on Numerical Methods in Fluid Mechanics, Paris, France, 3–7 July 1972; pp. 60–68.
36. Greenshields, C.J. *OpenFOAM Programmer's Guide*, 2.4.0 ed.; OpenFOAM Foundation: London, UK, 2015.
37. Somers, B. The Simulation of Flat Flames With Detailed and Reduced Chemical Models. Ph.D. Thesis, Technische Universiteit Eindhoven, Eindhoven, The Netherlands, 1994.
38. Smith, G.P. GRI-3.0. 2000. Available online: http://www.me.berkeley.edu/gri_mech/ (accessed on 14 December 2016).
39. Malik, M.R.; Vega, P.O.; Coussement, A.; Parente, A. Combustion modeling using Principal Component Analysis: A posteriori validation on Sandia flames D, E and F. *Proc. Combust. Inst.* **2020**, in press. [CrossRef]
40. Ren, S.; Wang, X. NOx emission and its reduction mechanism investigation in one diffusion-like vortex-tube combustor. *J. Clean. Prod.* **2020**, *274*, 123138. [CrossRef]
41. Gopal, A.; Volpiani, P.S.; Yellapantula, S.; Larsson, J. Computational investigation of real fluid effects in cryogenic laminar premixed CH4–O2 flames. *J. Supercrit. Fluids* **2020**, *168*, 105045. [CrossRef]
42. Fiolitakis, A.; Arndt, C. Transported PDF simulation of auto-ignition of a turbulent methane jet in a hot, vitiated coflow. *Combust. Theory Model.* **2020**, *24*, 326–361. [CrossRef]
43. Zhang, Q.; Chen, G.; Deng, H.; Wen, X.; Wang, F.; Zhang, A.; Sheng, W. Experimental and numerical study of the effects of oxygen-enriched air on the laminar burning characteristics of biomass-derived syngas. *Fuel* **2021**, *285*, 119183. [CrossRef]
44. Parente, A.; Sutherland, J.C.; Tognotti, L.; Smith, P.J. Identification of low-dimensional manifolds in turbulent flames. *Proc. Combust. Inst.* **2009**, *32*, 1579–1586. [CrossRef]
45. Pitsch, H.; Chen, M.; Peters, N. Unsteady flamelet modeling of turbulent hydrogen-air diffusion flames. *Symp. Combust.* **1998**, *27*, 1057–1064. [CrossRef]
46. Pitsch, H. Unsteady flamelet modeling of differential diffusion in turbulent jet diffusion flames. *Combust. Flame* **2000**, *123*, 358–374. [CrossRef]
47. Durand, L.; Polifke, W. Implementation of the thickened flame model for large eddy simulation of turbulent premixed combustion in a commercial solver. In Proceedings of the ASME Turbo Expo 2007: Power for Land, Sea, and Air. American Society of Mechanical Engineers, Montreal, QC, USA, 14–17 May 2007; pp. 869–878.
48. Schmitt, T.; Sadiki, A.; Fiorina, B.; Veynante, D. Impact of dynamic wrinkling model on the prediction accuracy using the F-TACLES combustion model in swirling premixed turbulent flames. *Proc. Combust. Inst.* **2013**, *34*, 1261–1268. [CrossRef]
49. Proch, F.; Kempf, A.M. Numerical analysis of the Cambridge stratified flame series using artificial thickened flame LES with tabulated premixed flame chemistry. *Combust. Flame* **2014**, *161*, 2627–2646. [CrossRef]
50. Scholtissek, A.; Chan, W.L.; Xu, H.; Hunger, F.; Kolla, H.; Chen, J.H.; Ihme, M.; Hasse, C. A multi-scale asymptotic scaling and regime analysis of flamelet equations including tangential diffusion effects for laminar and turbulent flames. *Combust. Flame* **2015**, *162*, 1507–1529. [CrossRef]
51. Claramunt, K.; Consul, R.; Carbonell, D.; Pérez-Segarra, C. Analysis of the laminar flamelet concept for nonpremixed laminar flames. *Combust. Flame* **2006**, *145*, 845–862. [CrossRef]
52. Cuoci, A.; Frassoldati, A.; Faravelli, T.; Ranzi, E. A computational tool for the detailed kinetic modeling of laminar flames: Application to C2H4/CH4 coflow flames. *Combust. Flame* **2013**, *160*, 870–886. [CrossRef]

53. Cuoci, A.; Frassoldati, A.; Faravelli, T.; Ranzi, E. Numerical modeling of laminar flames with detailed kinetics based on the operator-splitting method. *Energy Fuels* **2013**, *27*, 7730–7753. [CrossRef]
54. Cuoci, A.; Frassoldati, A.; Faravelli, T.; Ranzi, E. OpenSMOKE++: An object-oriented framework for the numerical modeling of reactive systems with detailed kinetic mechanisms. *Comput. Phys. Commun.* **2015**, *192*, 237–264. [CrossRef]
55. Auzillon, P.; Fiorina, B.; Vicquelin, R.; Darabiha, N.; Gicquel, O.; Veynante, D. Modeling chemical flame structure and combustion dynamics in LES. *Proc. Combust. Inst.* **2011**, *33*, 1331–1338. [CrossRef]
56. Delhaye, S.; Somers, L.; Van Oijen, J.; De Goey, L. Incorporating unsteady flow-effects in flamelet-generated manifolds. *Combust. Flame* **2008**, *155*, 133–144. [CrossRef]
57. Vreman, A.; Albrecht, B.; Van Oijen, J.; De Goey, L.; Bastiaans, R. Premixed and nonpremixed generated manifolds in large-eddy simulation of Sandia flame D and F. *Combust. Flame* **2008**, *153*, 394–416. [CrossRef]
58. Sacomano Filho, F.L.; Kuenne, G.; Chrigui, M.; Sadiki, A.; Janicka, J. A consistent Artificially Thickened Flame approach for spray combustion using LES and the FGM chemistry reduction method: Validation in Lean Partially Pre-Vaporized flames. *Combust. Flame* **2017**, *184*, 68–89. [CrossRef]
59. Ihme, M.; See, Y.C. LES flamelet modeling of a three-stream MILD combustor: Analysis of flame sensitivity to scalar inflow conditions. *Proc. Combust. Inst.* **2011**, *33*, 1309–1317. [CrossRef]